Engineering Science & Technology
http://ojs.wiserpub.com/index.php/EST/

UNIVERSAL WISER PUBLISHER

Research Article

Simulation of Automotive Components to Optimize Best Application from Different Grades of Steel Using Finite Element Method (FEM)

Amarjeet Kumar Singh*, D Satish Kumar

JSW Steel Ltd. Vijaynagar work, Bellary, Karnataka 583123, India
Email: amarjeet.singh1@jsw.in

Received: 25 September 2023; **Revised:** 1 April 2024; **Accepted:** 10 April 2024

Abstract: The automotive industry has been continuously striving to reduce weight in order to improve fuel efficiency and enhance safety. One approach to achieve this is by utilizing high-strength structural components. With each new model, automotive designers make changes to the structural components and material specifications to enhance efficiency and safety. Due to the availability of various high-strength steels with different formability characteristics, it is important to study and identify the most suitable grade of steel for different critical components. To determine the optimal and cost-effective grade of steel for specific applications, FEA-based models offer a cost-effective solution. In this study, a finite element analysis (FEA) model was developed using PAMSTAMP to simulate the forming process of the B-pillar and hood of a car. This model was used to conduct forming simulations of the B-pillar & hood components using six commonly used advanced high-strength steels (AHSS) in the automotive industry: DP590, DP780, DP980, DP1180, and CP780. The developed model predicted and compared potential crack locations, major/minor strains, stress distribution, and thinning profiles for the selected steel grades. The results revealed that DP590 exhibited a higher tendency for wrinkling, while DP980 and DP1180 showed a propensity for cracking at the bend section due to their lower formability. On the other hand, DP780 and CP780 were found to be ideal for the selected B-pillar & hood design. However, CP780 would require a higher blank force compared to DP780. Currently, this model is being utilized for the development of new steel grades and for assessing the suitability of design specifications offline. This reduces the need for physical experiments and enables more efficient advancements in the field.

***Keywords*:** finite element analysis (FEA), advanced high-strength steels (AHSS), B-pillar, PAMSTAMP

1. Introduction

Sheet metal forming is one of the most important processes in car manufacturing. Recent trends in car production may be characterized by the application of lightweight materials for auto structures, where the priority is to fulfil both the customers' demands and the increased legal requirements [1]. Lighter vehicles are desirable for consumers, who see a decline in the cost of ownership when fuel efficiency rises. A 10% decrease in vehicle weight is correlated with a 6-8% fuel efficiency increase [2].

The application of high-strength steels may be regarded as one of the potential possibilities. Applying high-strength steels has a positive response for many of the requirements: increasing the strength may lead to the application of thinner sheets resulting in significant mass reduction. Mass reduction is leading to lower fuel consumption with

DOI: https://doi.org/10.37256/est.5220243709

increased environmental protection. However, increasing the strength can often lead to a decrease in formability, which is very unfavourable for the forming processes as shown in Figure 1(a).

Lightweighting was traditionally viewed as a cost versus weight trade-off. Reducing the weight of the vehicle meant more expensive materials and more complicated manufacturing processes. The cost savings of the smaller drivetrain in internal combustion engine vehicles do not come close to making up for the cost increase from lightweighting in the body structure.

In the fulfilment of these manifold requirements, weight reduction has an important role: reducing the overall weight of vehicles results in lower consumption and thus less harmful emissions together with more economical vehicles and increased environmental protection. If we analyse the potential weight reduction in various parts of a regular automobile [2], [3], it can be seen that about 45% of the total weight is covered by the body parts, chassis, and suspension elements (Figure 1(b)); thus we have to focus on these components.

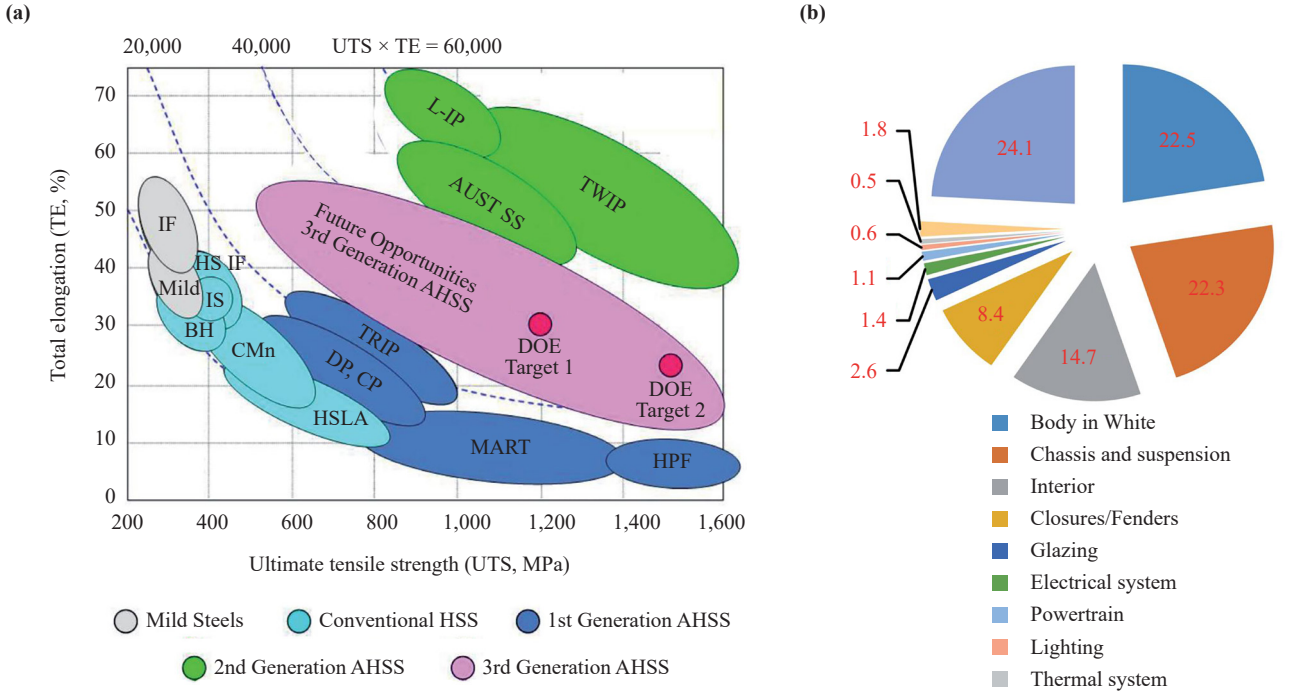

Figure 1. (a) Relationship between ultimate tensile strength (UTS) vs total elongation (TE) for various generations of high-strength steels [3]. (b) Weight ratio of various vehicle components [4], [5]

Hariharan et al. [3] examined the technical suitability and cost-effectiveness of austenitic steel for reducing the weight of a typical automotive component. They studied the forming behaviour of an Ashok Leyland ECOMET model bumper made of EDD steel and compared it with different grades of steel, namely TRIP and DP, based on various design factors. Peraprutchaya et al. [4] conducted simulations of forming and springback for an automotive roof component (Panel-RF FRT HRD) using PAM-STAMP software. Three different material models, namely the Y-U model, Hill's model, and the 980 GEN2 GPa model, were employed to analyse the springback effect. The authors concluded that the Y-U model is suitable for modelling springback. Silva et al. [5] performed experimental and numerical investigations on two automotive stamped parts: a rear seat and a structural reinforcement. Numerical simulations were carried out using the commercial finite element program PAM-STAMP. The paper also highlights the limitations of traditional build-and-test methods in developing a complete tool system and demonstrates how numerical modelling can help avoid costly die tryouts by providing accurate stamping analysis.

Asgari et al. [6] investigated the accuracy of finite element (FE) techniques in predicting the forming behaviour of

AHSS grades, such as TRIP and DP, compared to commonly used conventional steel grades. Three simulation methods, namely one-step, implicit, and explicit techniques, were employed to model the forming process of an automotive part. The results were correlated with experimental strain and thickness measurements of manufactured components from the production line. Yan et al. [7] simulated the Vehicle Cowl Inner Panel using the commercial FEA software DynaForm. The panel exhibits complex shape features, including bulges, reinforcing ribs, and holes. The authors studied the influence of binder force and fillet radii of the addendum surface on the occurrence of defects such as wrinkling, cracking, or incomplete forming.

You et al. [8] examined the effect of process and material variables on formability in the hot stamping process of actual automotive parts. The results demonstrated that the initial temperature and thickness of the sheet significantly affect formability. This study provides a practical approach to optimize the hot stamping process of mass-produced automotive body parts.

The present study aims to investigate the influence of different grades of steel on minor strain, thickness, and stress concentration through FEA simulations. This model can contribute to the development of new products, component design, and reduction in the need for physical experiments during the product development stage. Furthermore, the use of FEA simulations facilitates proper product development and component design, and reduces the requirement for physical experiments, resulting in a more efficient and cost-effective process. In conclusion, the FEA model is an indispensable tool for selecting appropriate materials in the automotive industry, offering an accurate and reliable method to analyze the impact of forming on different grades of steel and determine the most suitable material for specific components. By utilizing FEA simulations, the automotive industry can effectively address challenges related to formability, spring back, and joining, ultimately enhancing overall efficiency and product development quality.

2. Experimentation

2.1 *Material used*

The material used in this study was different grades of steel with a sheet thickness of 1.4 mm. The chemistry and mechanical properties of the material are given in Tables 1 and 2 respectively in as received condition.

Table 1. Chemical composition of different grades of materials used

Grade	Composition (%)								
	C	Mn	P	Si	Al	V	Mo	Nb	Ti
LA380	0.078	0.87	0.012	0.013	0.044	0.025		0.027	0.055
DP590	0.117	1.58		0.229				0.024	0.011
DP780	0.12	1.6	0.048	0.25	0.065	0.008	0.001	0.045	0.022
DP980	0.125	2.23	0.018	0.047			0.001	0.064	0.027
DP1180	0.125	2.23	0.018	0.423	0.047		0.001	0.064	0.027

Table 2. Mechanical properties of different grades of steel as received conditions

Grade	YS (MPa)	UTS (MPa)	n-Value	Elongation (%)
LA380	400	518	0.1296	25.4
DP590	438	602	0.129	24.6
DP780	545	826	0.202	17.4
DP980	674	1,025	0.183	13.9
DP1180	889	1,222	0.175	12.0

2.2 *Tensile test*

Tensile tests were performed at room temperature using an uniaxial tensile machine. To understand the flow behaviour of selected grades of steel tests were done in velocity control mode. Specimens are prepared using wire Electrical Discharge Machining (EDM) according to ISO III (JIS DIN 50125) standard as shown in Figure 2. All tensile tests were conducted using velocity control mode and the velocity of the tensile test was 0.008 mm/s.

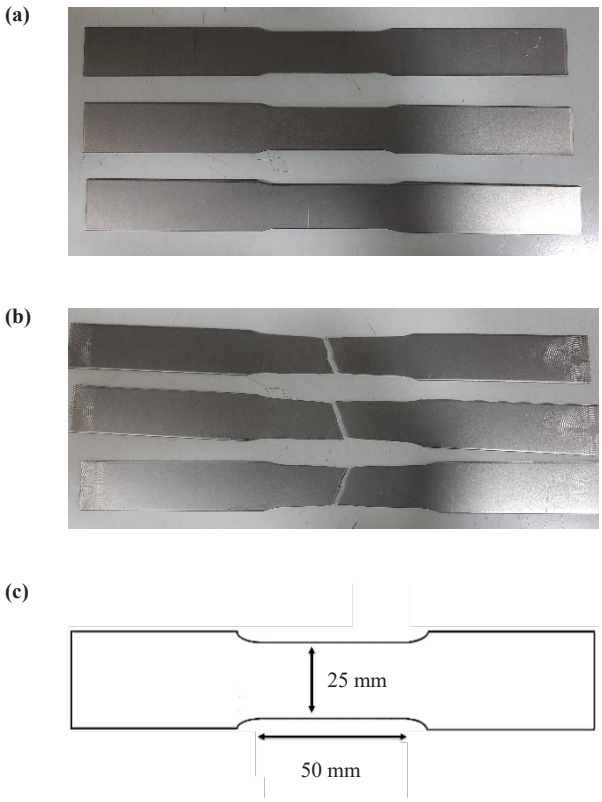

Figure 2. Tensile specimen (a) Initial and (b) after deformation conditions (c) Dimension used for experiment

2.3 *Formability test*

The forming limit diagram (FLD) experimental platform is utilized to offer various forming process parameters and boundary conditions whereas different geometries of specimens and boundary conditions involved in FLD experiments can force the limit strain measuring results to scattering and confusion. The punch, die, Digital Image Correlation (DIC) device, and lighting system were first integrated into the hydraulic press system. This experimental procedure and the device set-up conduce to rapid-integrated FLD measurement for all sheet metal forming.

In this paper, the Nakajima bulging test was chosen to determine the FLD of different grades of steel at room temperature and punch speed of 10 mm/s, and other parameters for conducting the test are given in Table 3. Integrated with DIC optical measuring system, the Nakajima device consists of an annular die with an inner diameter of 108 mm, a hemispherical punch with a diameter of 100 mm, and a blank holder with a pipe-section draw bead, as shown in Figure 3(a). The Teflon tape with grease was utilized to improve the interface lubrication between the punch and specimen in the bulging process. Teflon tape with a thickness of 1 mm was set on the specimen to reduce the friction effect and guide the fracture position close to the apex of the bulged dome. Besides, the DIC system was fixed flexibly under the Nakajima die to record the real-time deformation histories and calculate the strain fields of specimens. The major and minor strains of the FLD were obtained by using inverse parabolic fitting according to the position-dependent method specified in ISO 12004-2:2008.

During the bulging process, the specimen was firmly clamped by the blank holder and then bulged to fracture by the punch at a designated speed. Finally, the limit strains of different specimens were calculated by the analysis software GOM-Correlate in the post-process.

The formability test was conducted using ISO 12004-2:2008 standard. To conduct the experiments eight specimens were prepared using wire-EDM as shown in Figure 3. Eight blanks of different widths varying from 25 mm to 200 mm with the same lengths of 200 mm were used to capture the different strain paths. Test specimens with different dimensions were designed referring to the ISO 12004-2:2008 standard, as shown in Figure 3. Seven variant widths are chosen in this work, including 20 mm, 45 mm, 70 mm, 95 mm, 120 mm, 145 mm, and 170 mm.

(a)

(b)

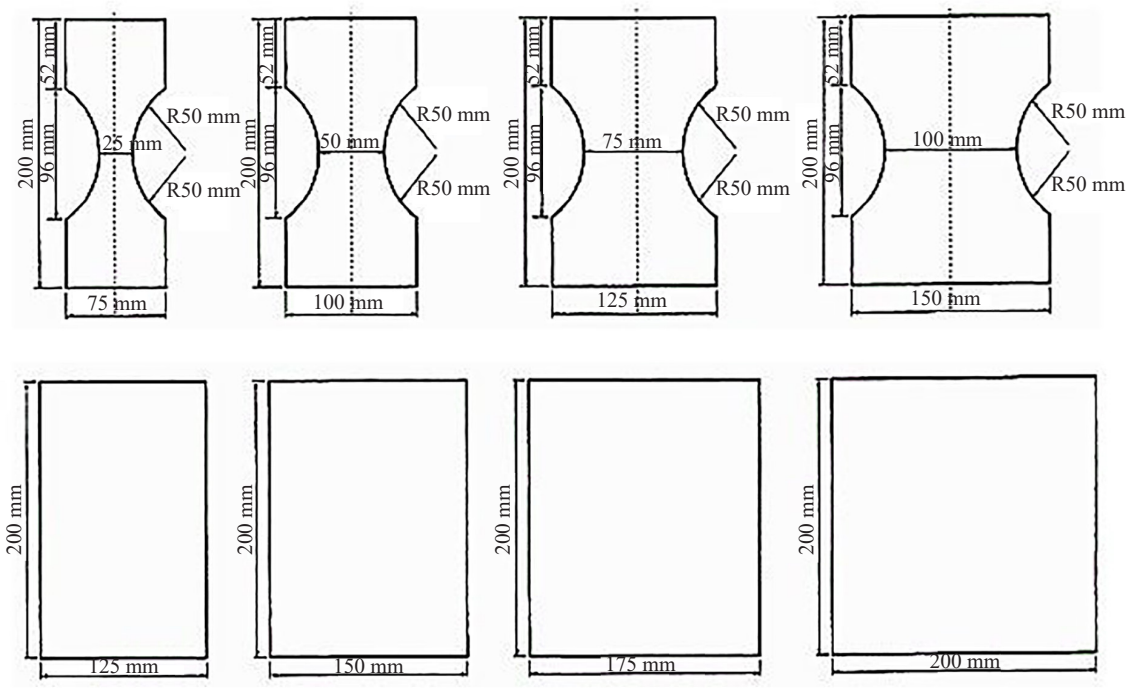

(c)

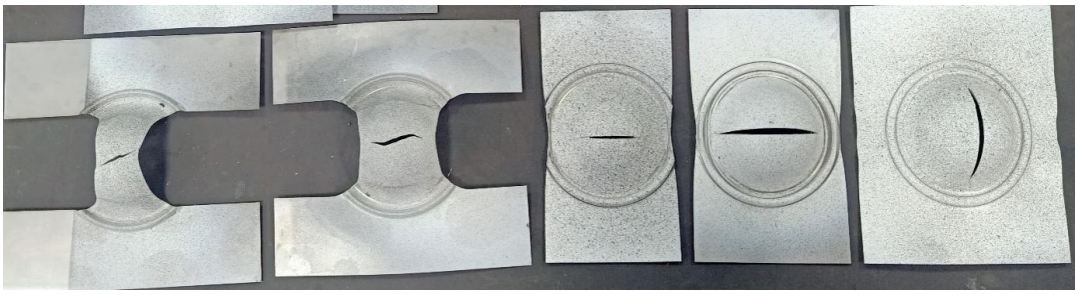

Figure 3. (a) Deep drawing experimental apparatus used for formability determination using ISO Standards (b) Dimension for different used for Nakazima test (c) Deformed specimen

Table 3. Experimental Parameters for FLD Test

Parameters	Blank holding Force	Punch Velocity	Dimensions of specimen
Values	200 kN	10 mm/s	as per ISO standard

2.4 *FEM Simulation*

To optimize different grades of steel as mentioned in the previous section was selected as input materials for simulation work. To optimize the best materials, two automotive components, i.e., B-pillar and Cross-member were selected for this study. Finite Element Method (FEM) simulation was performed using PAMSTAMP software.

PAMSTAMP supports several types of meshing for creating model geometry. In the current problem, the geometry

of the die and punch are considered discrete rigid bodies with rigid 3D four nodded type mesh elements. The blank is assumed a deformable body with four nodded quadrilateral shell elements.

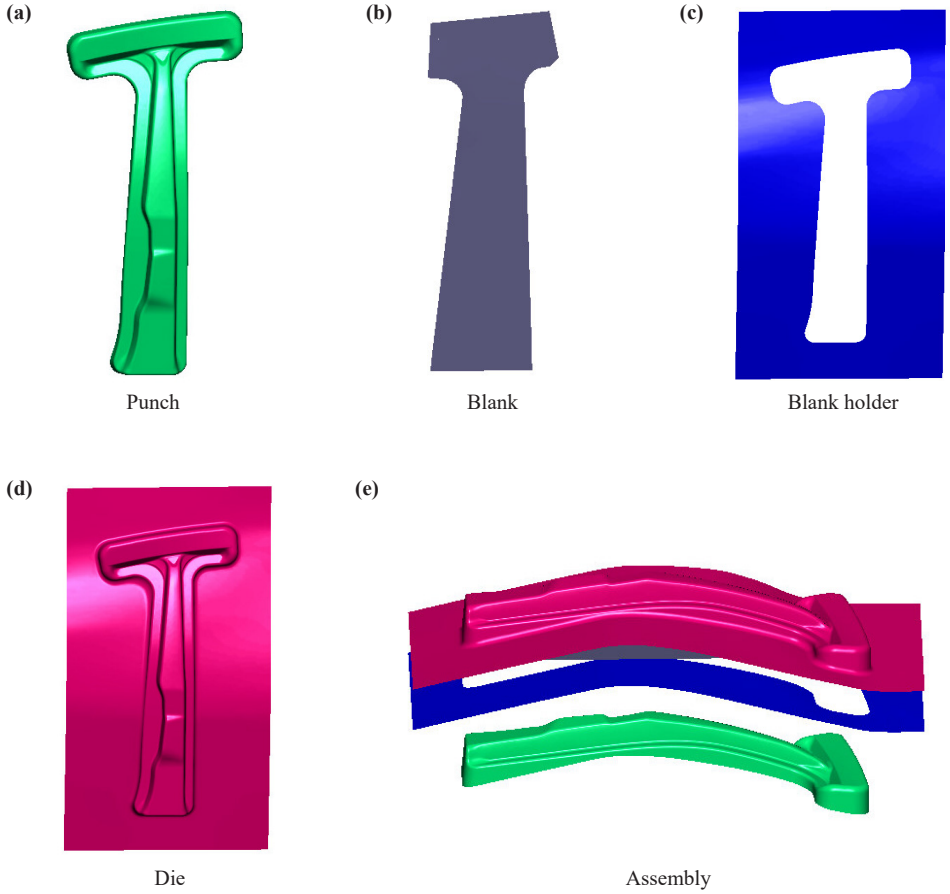

Figure 4. Die, Punch, Blank, Blank holder, and assembly of component used for B-pillar simulation in PAMSTAMP

To obtain the flow behaviour of materials, tensile tests were performed at room temperature; and for Forming Limit Curves (FLC), Nakazima tests were conducted. These two datasets were used as input for PAMSTAMP for simulation work.

Different material models were created for each material. For the determination of FLCs with incorporated strain rate dependant behaviour, material models were created with tabular data providing stress as a function of plastic strain and strain rate. Hardening behaviour was inputted as a lookup table of true stress and true strain. The material was assumed to be normal isotropic.

During the simulation, general CAD geometries were used for punch, die tool, blank holder, and blanks of different widths as shown in Figure 4 and Figure 5. Various other process parameters were provided with the values within the conventional ranges, i.e., friction coefficient of 0.125. All the parts were assumed to be rigid except blank. Mesh size was decided according to the accuracy needed. Fine mesh leads to more accuracy with more processing time and the reverse is true for coarse mesh. Here 1 mm^2 mesh of shell elements was provided with a maximum of 4 levels of refinement. Punch velocity and constant blank holding force were kept the same in all the simulations. Punch stroke was varied according to the strength and the type of loading, e.g., uniaxial, biaxial, or pure shear.

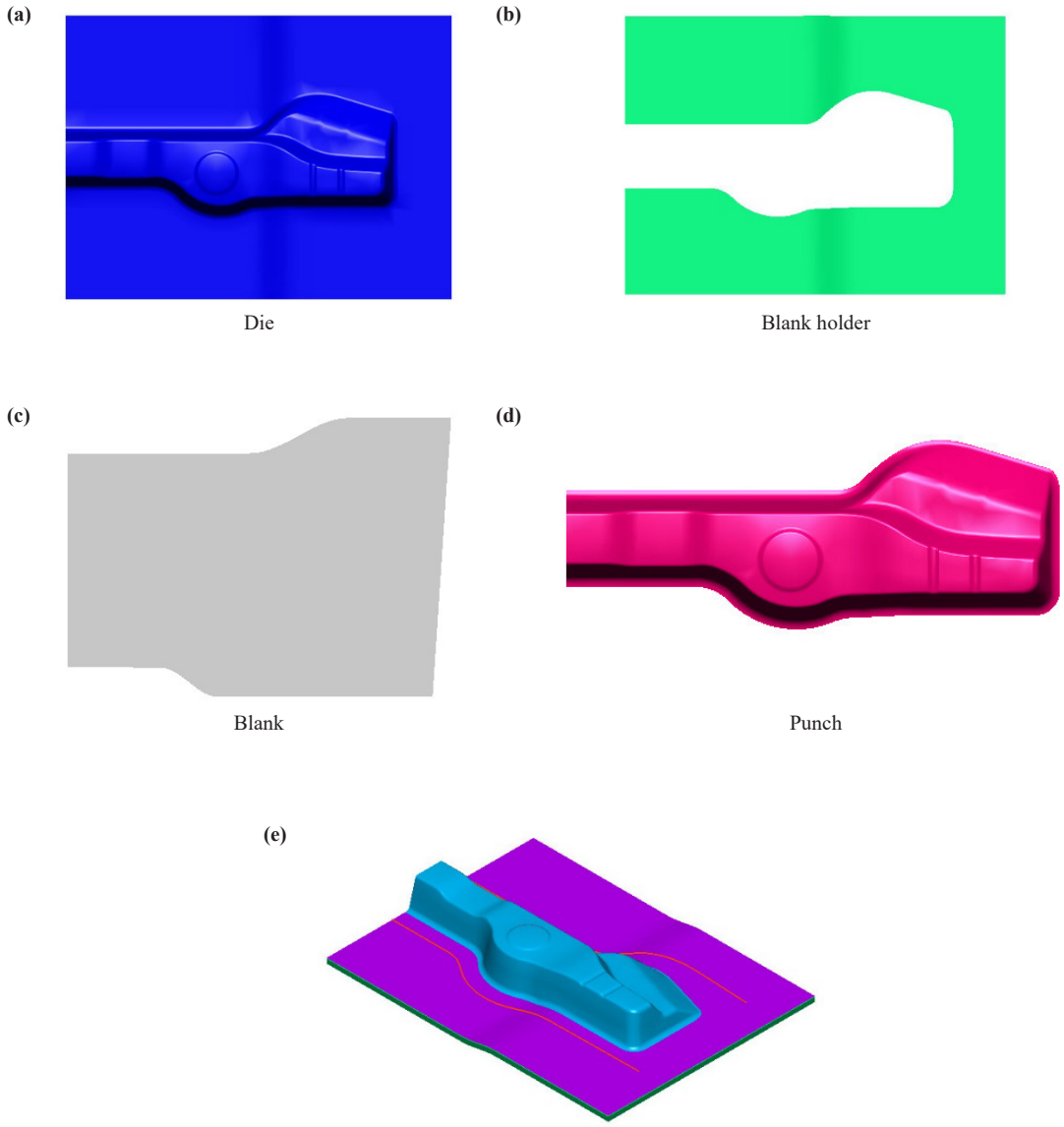

Figure 5. Die, Punch, Blank, Blank holder, and Assembly of component used for Cross-member simulation in PAMSTAMP

Setting up a simulation of a B-pillar and cross-member in PAM-STAMP software involves several steps:

Create the geometry: The geometry of the B-pillar and cross-member was imported as a CAD file into PAM-STAMP for simulation.

Material definition: Define the material properties for the B-pillar and cross-member for all selected grades.

Loads and Boundary conditions: Define the loads of 200 kN applied to the B-pillar and cross-member during the simulation. Once the load is defined, the positions of different components are established. Initially, the die is fixed, the blank is positioned on the die, and the movement of the blank and blank holder is restricted in all directions except the z-direction. However, the punch moves in the z-direction with a velocity of 10 mm/s.

Mesh generation: Once the geometry, material properties, and loads have been defined, a mesh for the B-pillar and cross member is generated. Here 1 mm^2 mesh of shell elements was provided with a maximum of 4 levels of refinement.

Solve: After the mesh had been generated, a simulation was run to solve for the stress and deformation of the b-pillar and cross member under the specified loads.

Results post-processing: Finally visualize and analyse the results of the simulation, including the stress, deformation distributions, and strains.

3. Result & discussion

3.1 *Tensile test*

Tensile testing is an important tool for evaluating the mechanical properties of different materials, including advanced high-strength steels (AHSS) used in automotive applications. In the case of AHSS, tensile strength, yield strength, and elongation are critical factors that determine the performance of the material under stress. The results of tensile tests for DP 590, DP 780, DP 980, DP 1180, and LA 380 show that these materials exhibit varying levels of strength and ductility. DP 590 has a tensile strength of around 602 MPa, while DP 780, DP 980, and DP 1180 have increasingly higher tensile strengths, with values of around 826, 1,025, and 1,222 MPa, respectively. Meanwhile, LA 380 has a lower tensile strength of around 518 MPa. These materials also exhibit varying levels of ductility, with DP 590, DP 780, and LA 380 showing higher elongation values compared to DP 980 and DP 1180 as shown in Figure 6. Overall, the results of tensile tests provide important insights into the mechanical properties of these AHSS materials and can inform the selection and design of components in automotive applications.

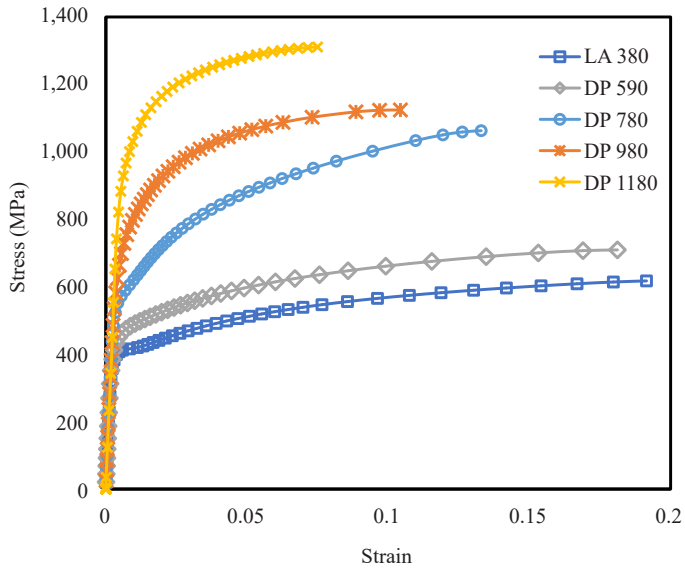

Figure 6. True stress vs true strain for different grades of steel at room temperature

The strain hardening exponent (also called the strain hardening index), usually denoted n, is a constant often used in calculations relating to stress-strain behaviour in work hardening. It occurs in the formula known as Holloman's equation which originally posited it.

$$\sigma = K\varepsilon^n$$

where sigma (σ) represents the applied true stress on the material epsilon (ε) is the true strain, and K is the strength coefficient. The value of the strain hardening exponent lies between 0 and 1, with a value of 0 implying a perfectly plastic solid and a value of 1 representing a perfectly elastic solid. Most metals have an n-value between 0.10 and 0.50.

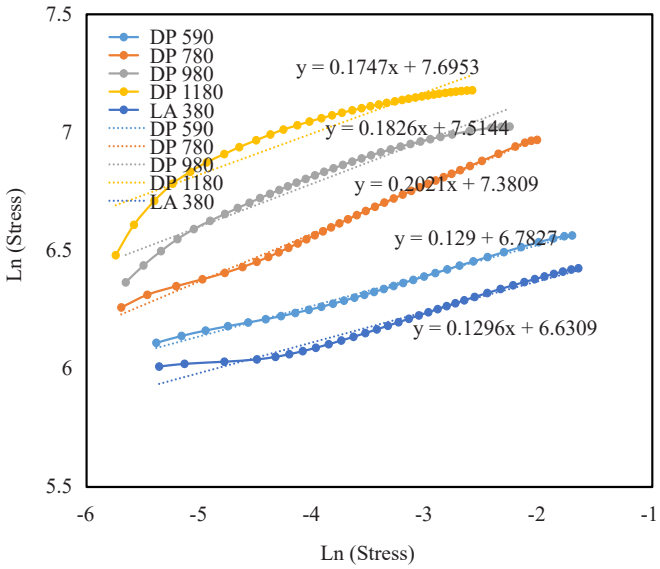

Figure 7. n-value for different grades of steel at room temperature

For selected grades of steel, the n-value is calculated as shown in Figure 7. It was observed that DP 780 had the highest strain hardening exponent compared to another grade of steel, however, a minimum value is observed for DP 1180. The numerical value of the strain hardening exponent is 0.202 for DP 780 steel. A detailed comparison is also given in Table 2. It was observed that the tensile test rate (strain rate) had an effect on the flow behaviour of materials at elevated temperatures for AHSS grade steel. Therefore, it was not considered in this work. However, the strain rate sensitivity index (m) had not much effect on ferrous (iron, steel) materials at room temperature whereas it affected non-ferrous materials (Al, Cu, etc.).

3.2 *Formability test*

A forming limit diagram, also known as a forming limit curve, is used in sheet metal forming to predict forming behaviour of sheet metal. The diagram attempts to provide a graphical description of material failure tests, such as a punched dome test [9], [10].

In order to determine whether a given region has failed, a mechanical test is performed. The mechanical test is performed by placing a circular mark on the workpiece prior to deformation and then measuring the post-deformation ellipse that is generated from the action on this circle. By repeating the mechanical test to generate a range of stress states, the formability limit diagram can be generated as a line at which failure is onset.

The semi-axes of the ellipse formed in this circle allow for the measurement of relative strain in two primary directions, known as the major and minor directions, which correspond to the major and minor semi-axes of the ellipse. Under the assumption of path-independent strain, the relative strains will reach a critical value at which deformations occur. Through repeated measurements, the shape of the curve can be obtained experimentally. Alternately, a formability limit diagram can be generated by mapping the shape of a failure criterion into the formability limit domain. However, the diagram is obtained, and the resultant diagram provides a tool for the determination of whether a given cold-forming process will result in failure or not. Such information is critical in the design of forming processes and is therefore fundamental to the design of sheet metal forming processes. Through the establishment of forming limit diagrams for a range of alloys, the forming process and alloy behaviour can be matched at the metalworking design time by the process engineer. Major strain vs minor strain for different selected grades of steel is shown in Figure 8. It was also observed that the formability of LA 380 was highest among the others whereas DP 1180 had the lowest major and minor strain.

In order to verify the simulation initially, the tensile test was validated using a developed model. After that FLC curves were validated using the same model. In the end, automotive components were simulated.

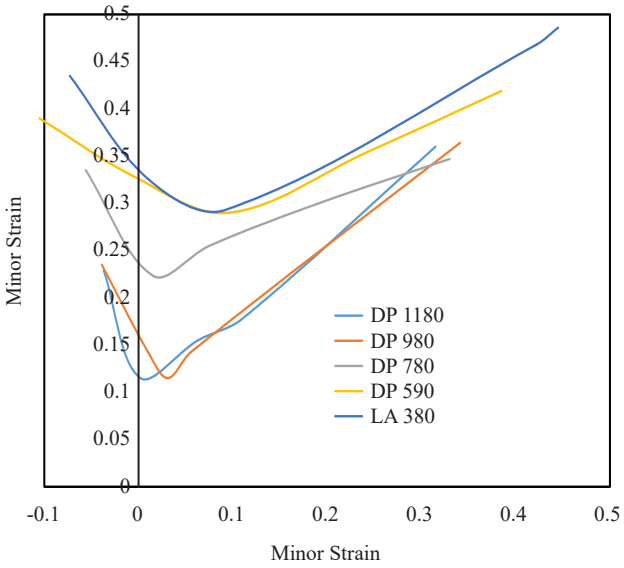

Figure 8. Major strain vs minor strain (Forming limit diagram) for different grades of steel

3.3 *FEM simulation*

Simulation makes it possible to detect errors and problems, such as wrinkles or splits in parts, on the computer at an early stage by using two parameters called thinning and formability. Therefore, in this work, FEM simulations were performed using PAMSTAMP. To simulate different grades of steel, two components, B-pillar and cross-member, were selected. Thickness, thinning, and stress distribution are discussed for both the components in the below sections.

3.3.1 *Thickness distribution in B-pillar*

The thickness distribution in a B-pillar is a critical factor in determining its strength and stiffness. The thickness of the B-pillar should be designed to provide enough strength to resist the loads it will be subjected to while also ensuring that it is not too heavy and does not compromise the overall weight of the vehicle.

In general, the thickness of the B-pillar will be thicker near the bottom where the compressive loads are highest and thinner near the top where the tensile loads are highest. This allows for a more efficient distribution of material, with more material in the areas where it is needed most.

In addition to the distribution of thickness, the shape of the B-pillar can also have an impact on its strength and stiffness. For example, a B-pillar with a U-shaped cross-section can provide improved rigidity compared to a rectangular cross-section, as it offers more resistance to bending.

It is important to note that the thickness distribution in the B-pillar should also be optimized in consideration of the material used. For example, a B-pillar made of a high-strength steel alloy can be made thinner compared to a pillar made of conventional steel due to its improved strength properties.

In conclusion, the thickness distribution in a B-pillar is a key design consideration that can impact the overall strength, stiffness, and weight of the vehicle. It should be optimized in consideration of the loads it will be subjected to, the material used, and the desired performance characteristics of the vehicle.

The thickness distribution for selected grades of steel is shown in Figure 9. It was observed that the best suitable material according to thickness variation is DP 780, whereas the worst material is DP 1180.

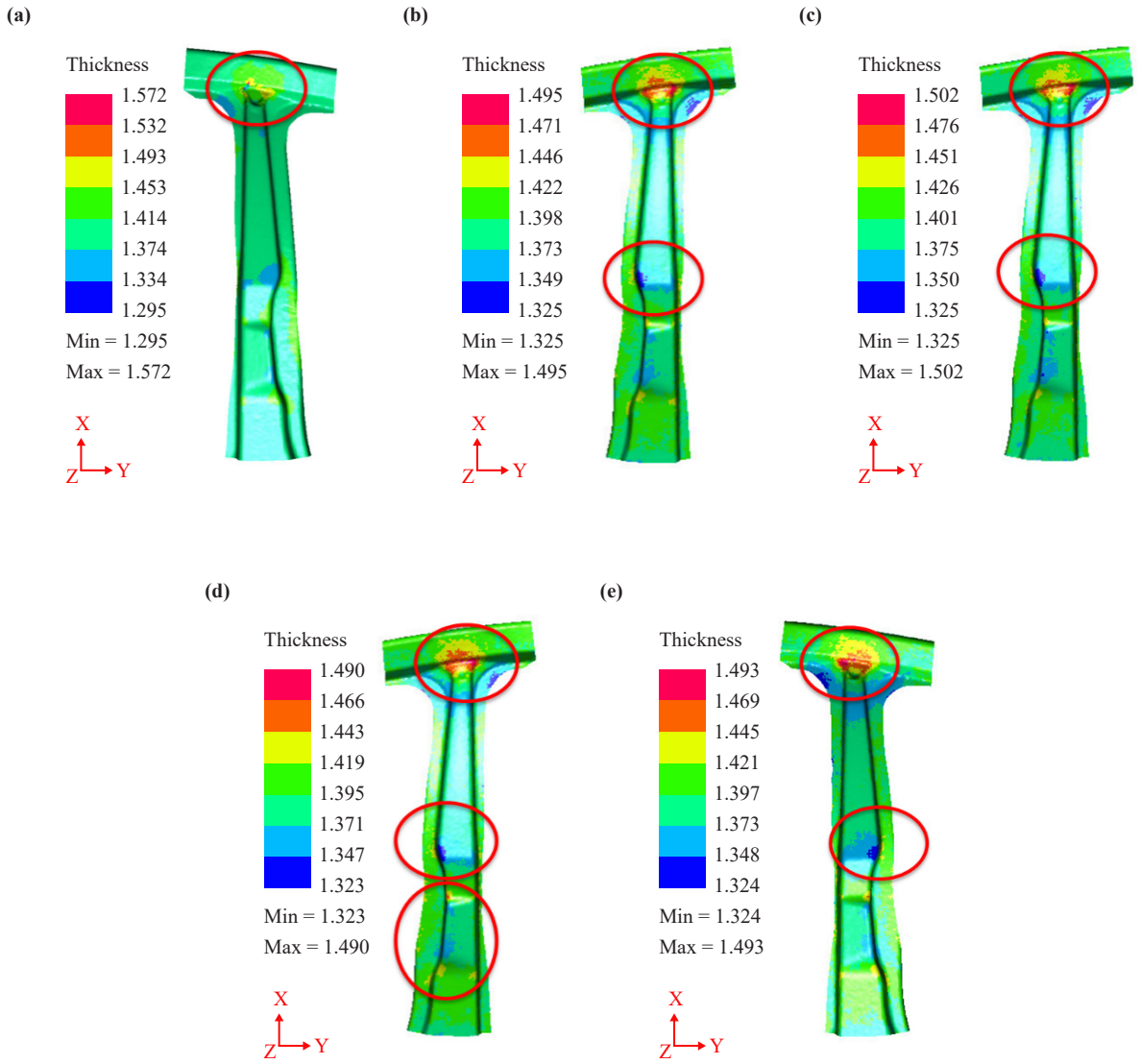

Figure 9. Thickness distribution in B-pillar for different grades of steel (a) DP 590 (b) DP 780 (c) DP 980 (d) DP 1180 (e) LA 380

3.3.2 *Thinning distribution in B-pillar*

The thinning distribution of the B-pillar is shown in Figure 10. It was observed that maximum thinning occurs in the neck zone of the B-pillar. It was found that maximum thinning occurs in DP 1180 whereas minimum thinning occurs in DP 780. It can also be concluded that the thinning distribution is uniform in DP 780 compared to other grades of steel.

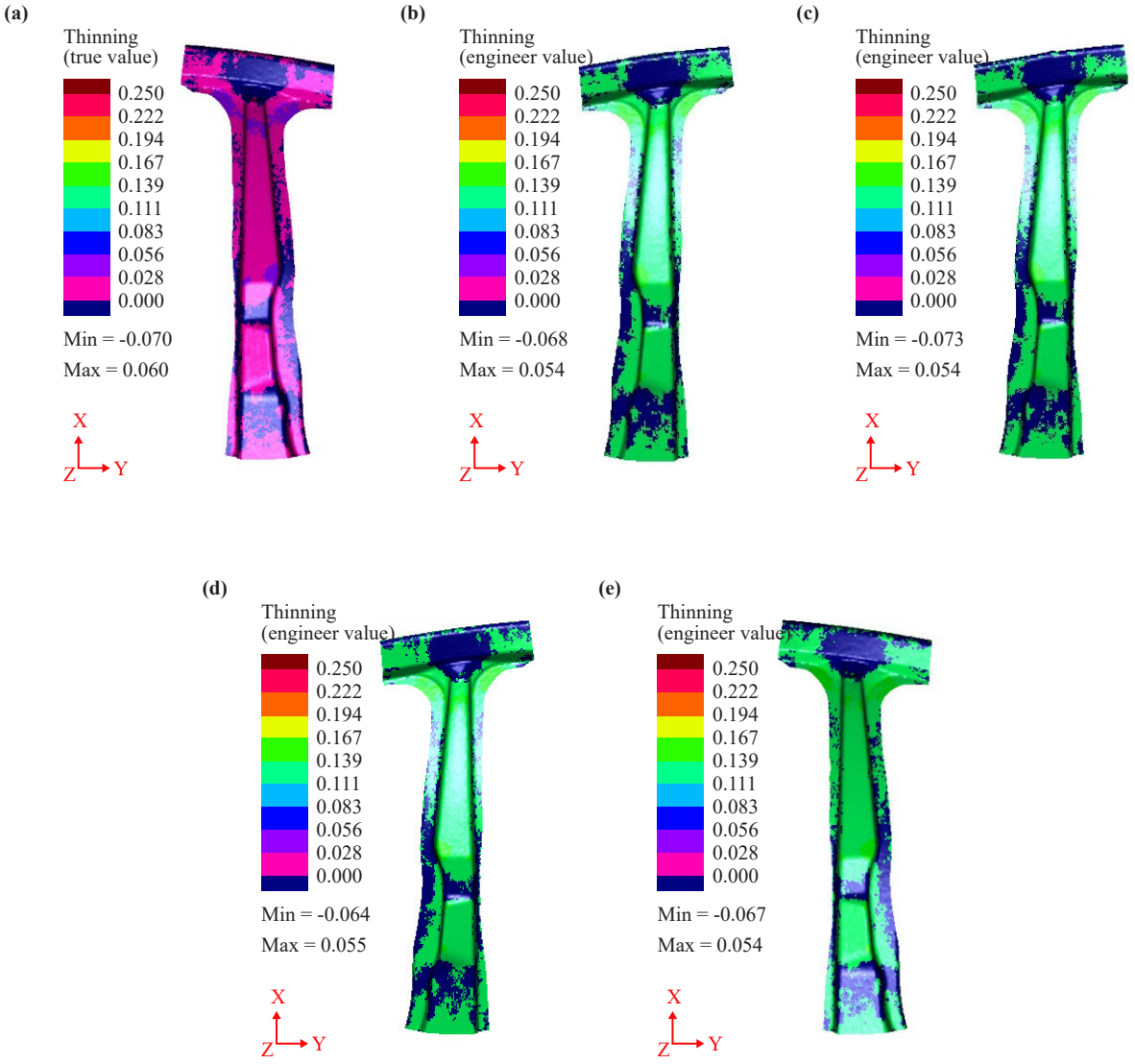

Figure 10. Thinning distribution in B-pillar for different grades of steel (a) DP 590 (b) DP 780 (c) DP 980 (d) DP 1180 (e) LA 380

3.3.3 *Stress distribution in B-pillar*

The stress distribution in a B-pillar refers to the way in which the applied loads are distributed throughout the material of the pillar. The B-pillar is an important structural component of a vehicle, providing stability and support to the vehicle body.

The stress distribution in a B-pillar is influenced by several factors, including the material properties of the steel used, the geometry and dimensions of the pillar, and the loads being applied to the pillar. The choice of steel grade will have an impact on the stress distribution, as different grades of steel have different mechanical properties and capabilities to withstand stress and fatigue loading.

The stress distribution in a B-pillar, also known as a centre pillar or middle pillar, depends on several factors including the design of the pillar, the material used, the loads acting on the pillar, and the type of loads.

In a vehicle, the B-pillar provides lateral support for the roof and is subjected to both compressive and bending loads. The distribution of stress within the B-pillar is complex and influenced by several factors including the location and magnitude of the loads, the stiffness of the structure, and the material properties of the pillar.

For a uniform load acting on the roof, the maximum compressive stress will occur at the bottom of the B-pillar,

while the maximum tensile stress will occur at the top of the pillar. However, the exact distribution of stress will depend on the geometry of the pillar and the specific loads acting on it.

In general, it is important for the B-pillar to be designed to withstand the loads it will be subjected to while also providing sufficient strength to protect occupants in the event of a collision. The material used for the B-pillar will also play a role in the stress distribution, with materials such as high-strength steel and aluminum providing good strength-to-weight ratios and improved crashworthiness.

Major stress distribution in the B-pillar is shown in Figure 11. It was observed that stress developed in the grade is more and less the same. However, according to strength best material used for the B-pillar is DP 1180 but with respect to ductility, it may be rejected. Therefore, in concluding remark best on the parametric studies best suitable material for B-pillar is DP 780.

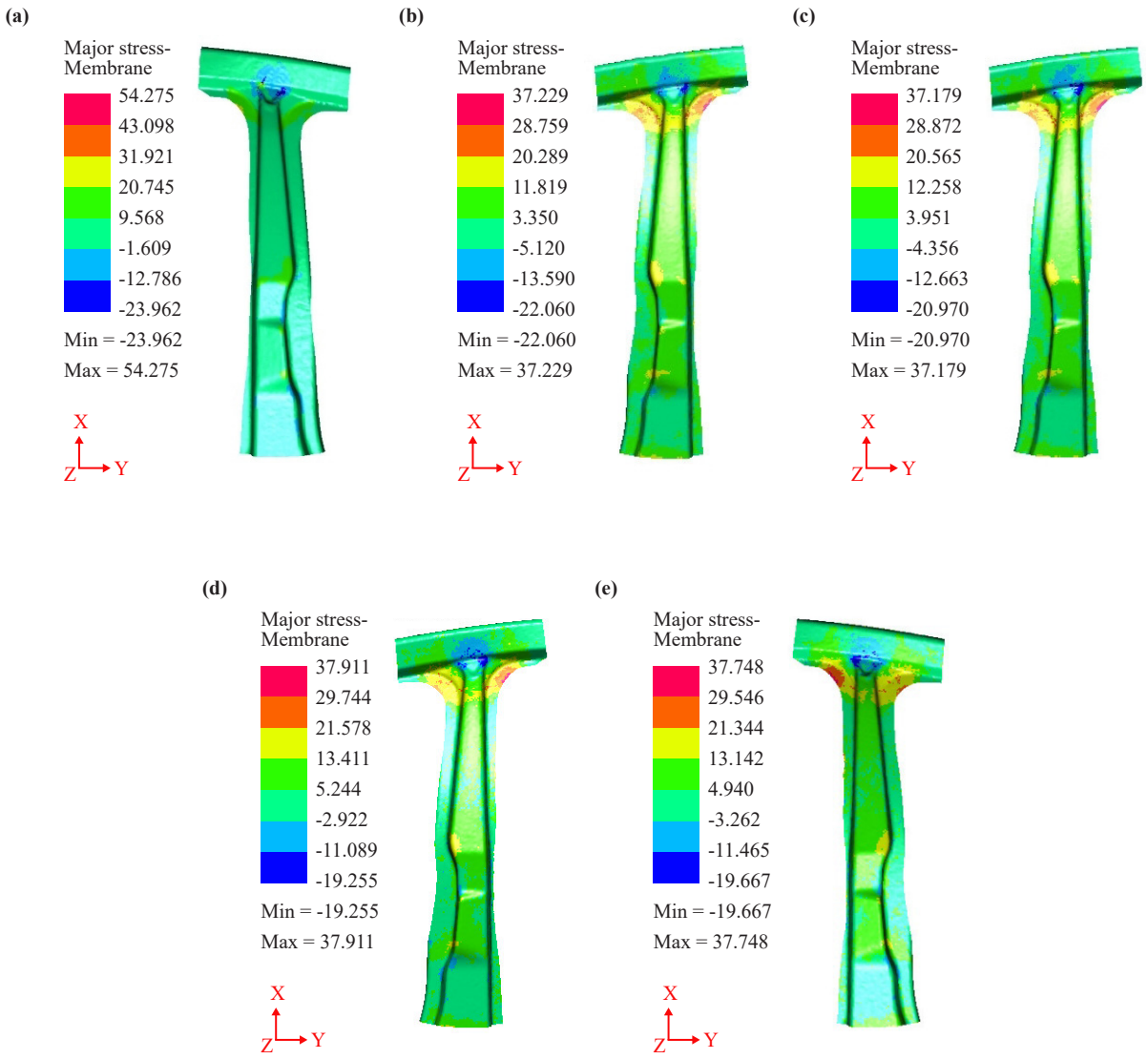

Figure 11. Major Stress distribution in B-pillar for different grades of steel (a) DP 590 (b) DP 780 (c) DP 980 (d) DP 1180 (e) LA 380

3.3.4 *Forming limit diagram in B-pillar*

A forming limit diagram (FLD) is a graphical representation of the conditions under which a material can undergo

plastic deformation without failure. The FLD shows the maximum strain that can be applied to a material in different directions without causing necking or fracture.

The forming limit diagrams of DP 590, DP 780, DP 980, DP 1180, and LA 380 steels can be determined through experiments or numerical simulations. The specific FLD of a particular grade of steel will depend on the material's microstructure, chemical composition, and other factors.

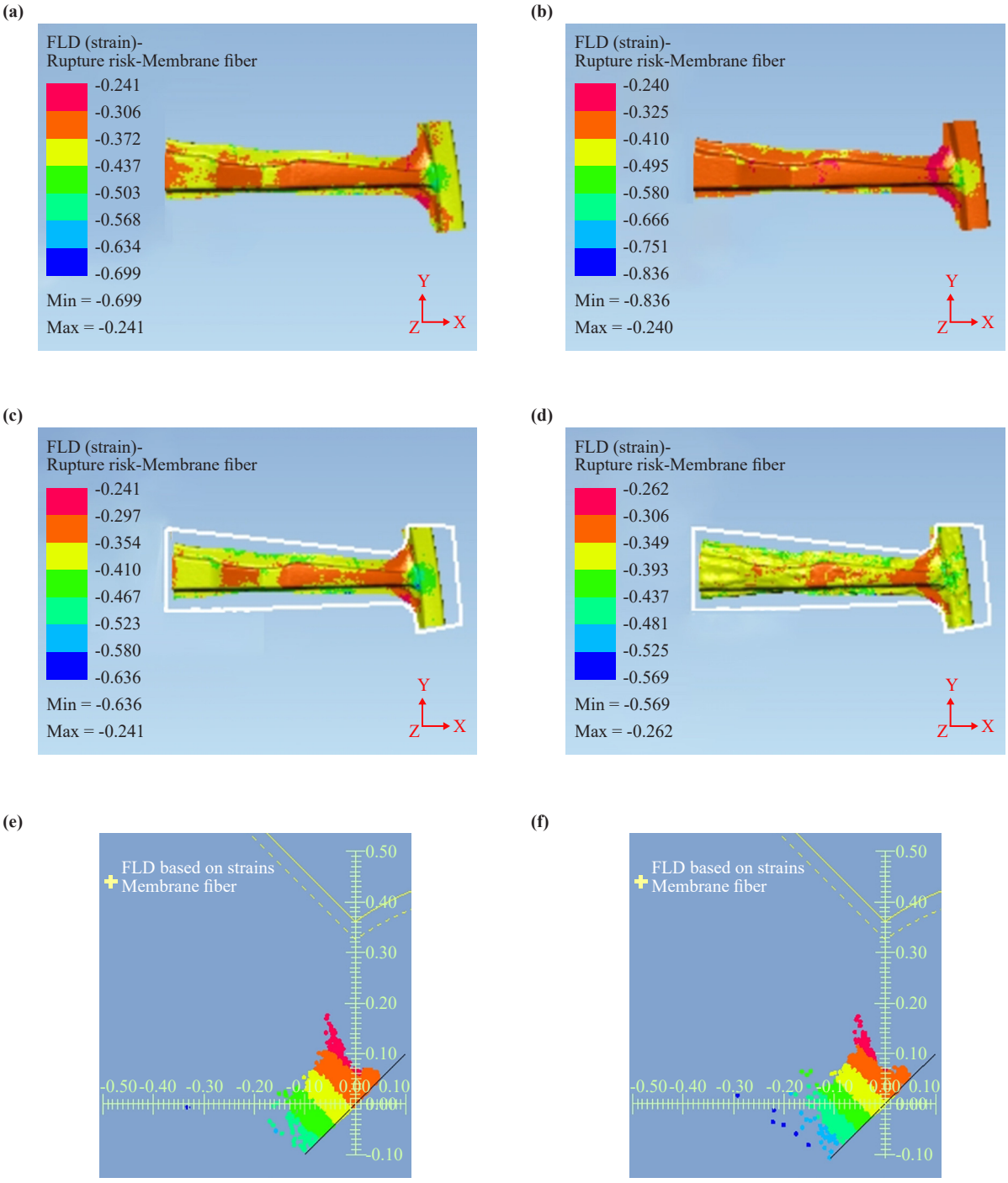

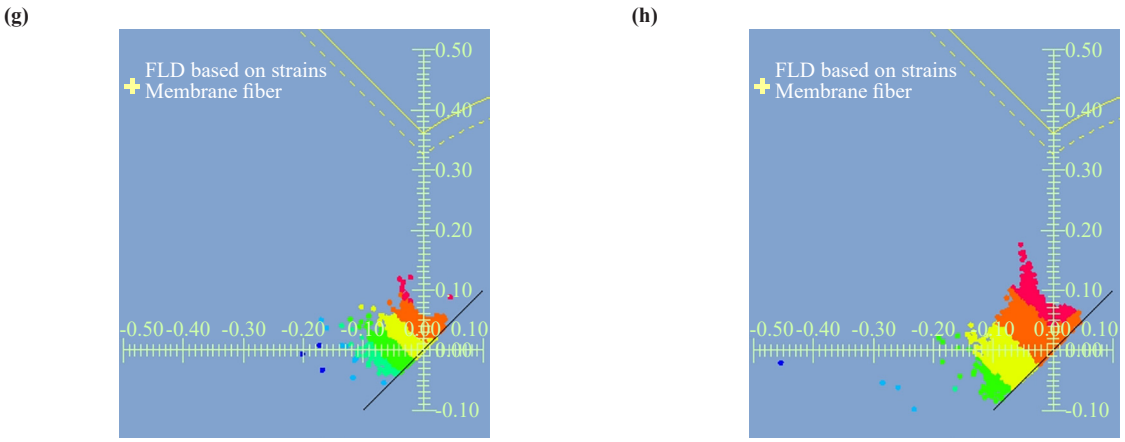

Figure 12. FLC and failure of B-pillar Component based on rapture criterion

In general, FLDs for advanced high-strength steels such as DP and LA steels tend to be more complex than those for conventional steels, due to the presence of multiple phases in their microstructure. The FLD for a specific grade of steel can be used to optimize the design and process of forming operations, such as stamping, deep drawing, and hydroforming, to achieve the desired properties and performance.

It is important to note that the forming limit diagrams for DP 590, DP 780, DP 980, DP 1180, and LA 380 steels can vary widely depending on the specific conditions of each case [11]. It is always recommended to consult the manufacturer's datasheet or conduct experiments or simulations to determine the accurate FLD for a particular grade of steel.

According to the rupture criterion, FLC curves were plotted for all grades of steel for the B-pillar component as shown in Figure 12. It was observed for FLC that maximum strain distribution is in the drawing region. Whereas some data points are in the 3rd quadrant of FLC indicating that both the major and minor strain values are negative in nature.

3.3.5 *Stress distribution in cross-member*

The stress distribution in a cross member refers to the distribution of stresses throughout the material due to the applied loads. The choice of steel grade will have an impact on the stress distribution in a cross member, as different grades of steel have different mechanical properties and capabilities to withstand stress and fatigue loading. Stress distribution for cross-members is shown in Figure 13.

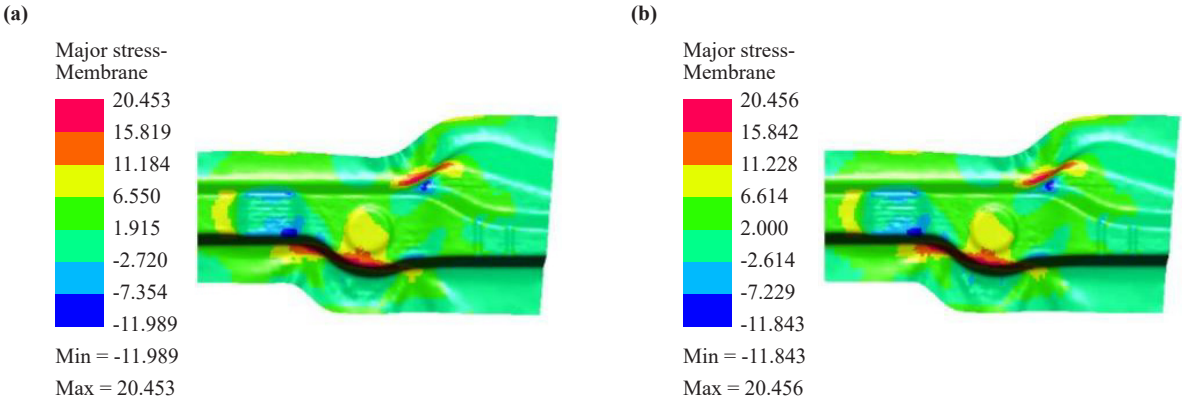

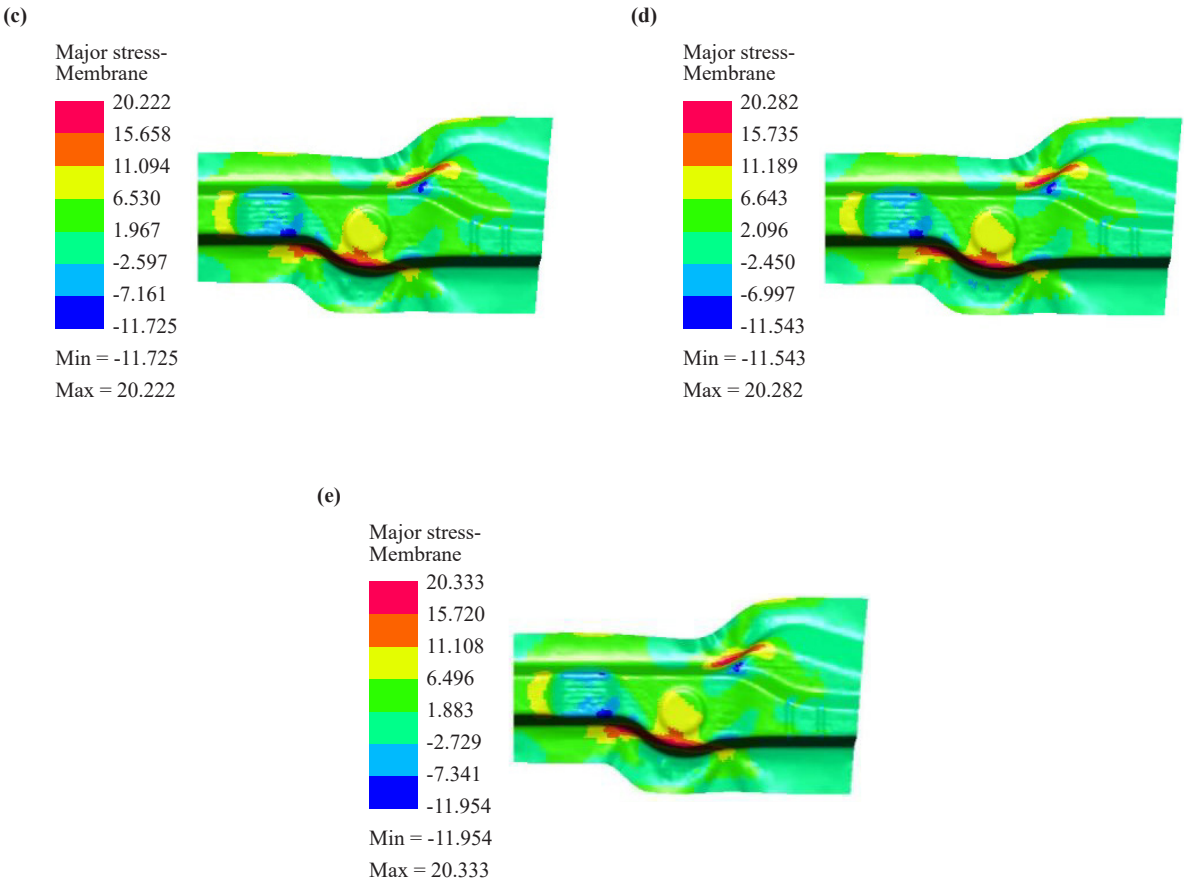

Figure 13. Major Stress distribution in cross members for different grades of steel (a) DP 590 (b) DP 780 (c) DP 980 (d) DP 1180 (e) LA 380

3.3.6 *Thickness distribution in cross-member*

The thickness distribution in cross members is shown in Figure 14. The thickness distribution in a cross member refers to the distribution of material thickness along the length or across the width of the member. The choice of steel grade will have a significant impact on the thickness distribution, as different grades of steel have different mechanical properties and capabilities to withstand stress and fatigue loading.

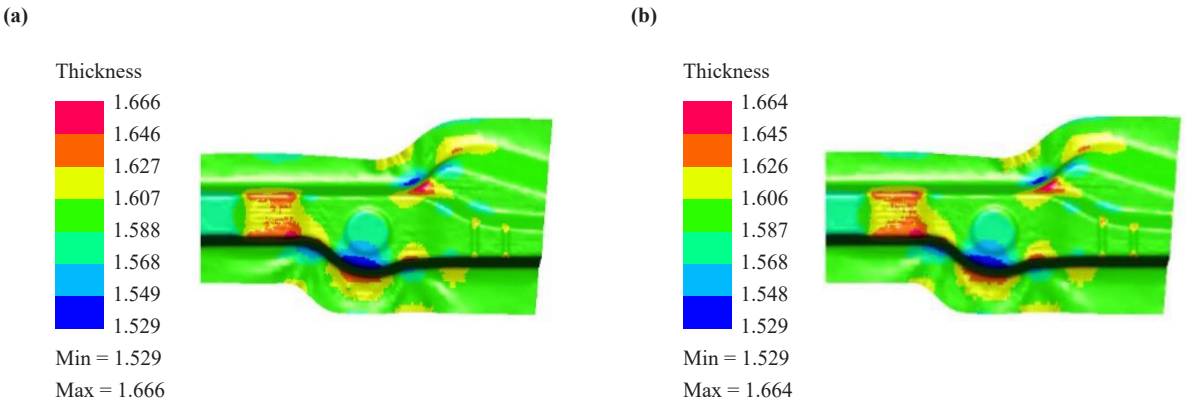

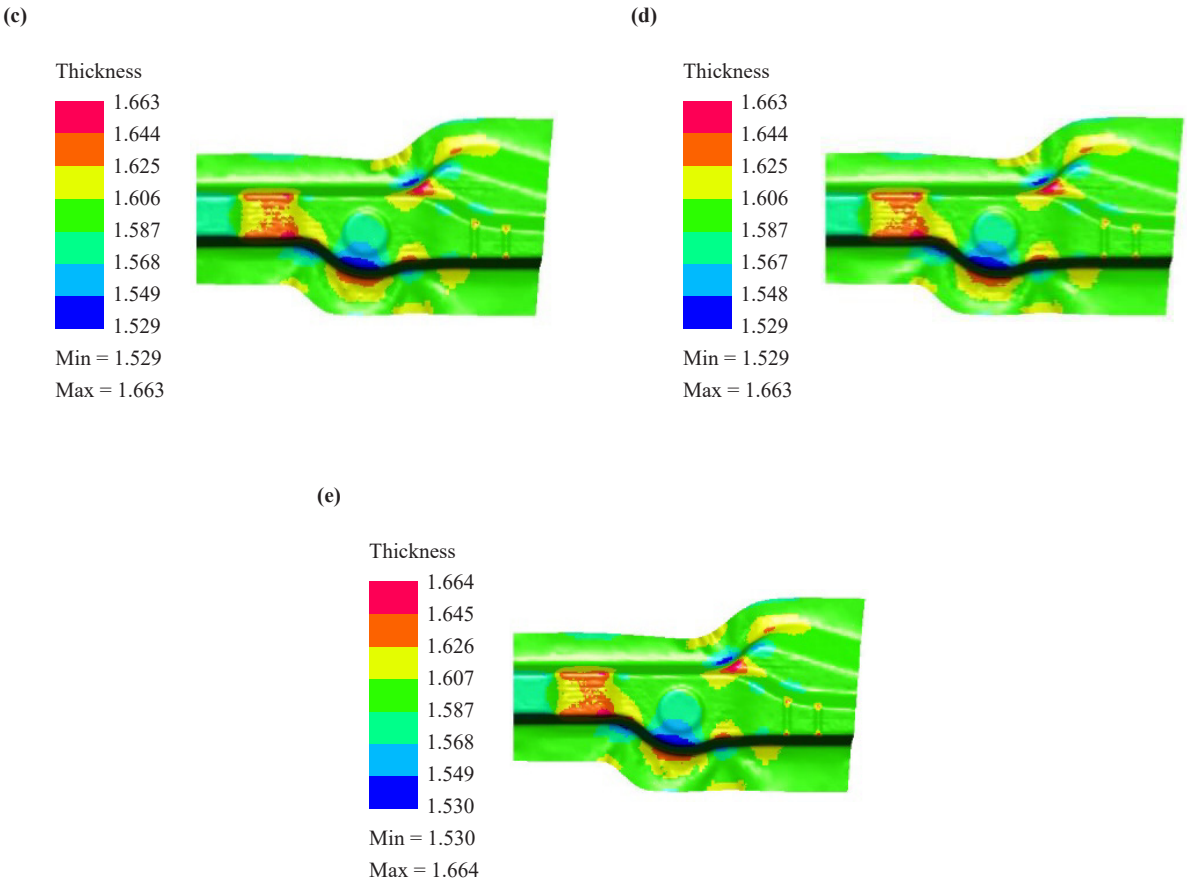

Figure 14. Thickness distribution in cross members for different grades of steel (a) DP 590 (b) DP 780 (c) DP 980 (d) DP 1180 (e) LA 380

3.3.7 *Thinning distribution in cross-member*

The thinning distribution in a cross member refers to the reduction in the thickness of the material in specific areas as shown in Figure 15, which is a common design consideration for structural members subjected to high stress and fatigue loading. The choice of steel grade for a cross member will have an impact on the thinning distribution, as different grades of steel have different mechanical properties and capabilities to withstand stress and fatigue loading.

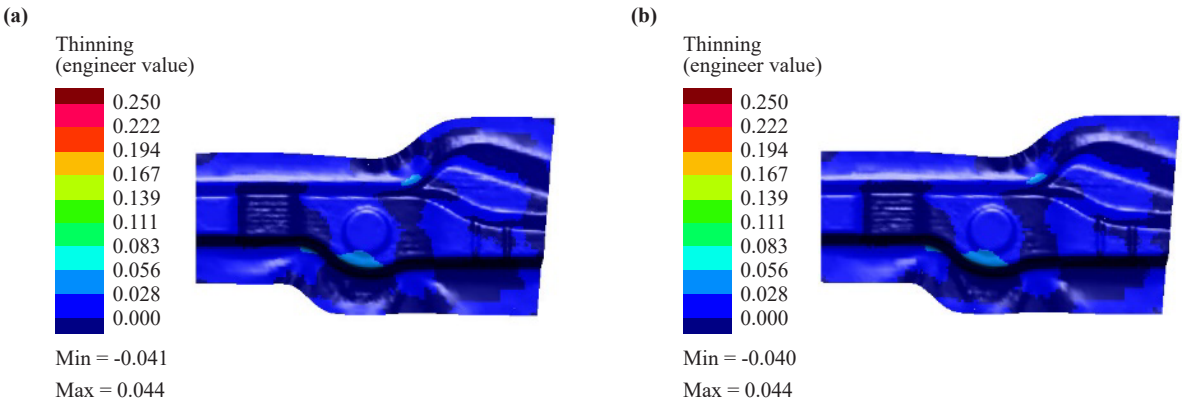

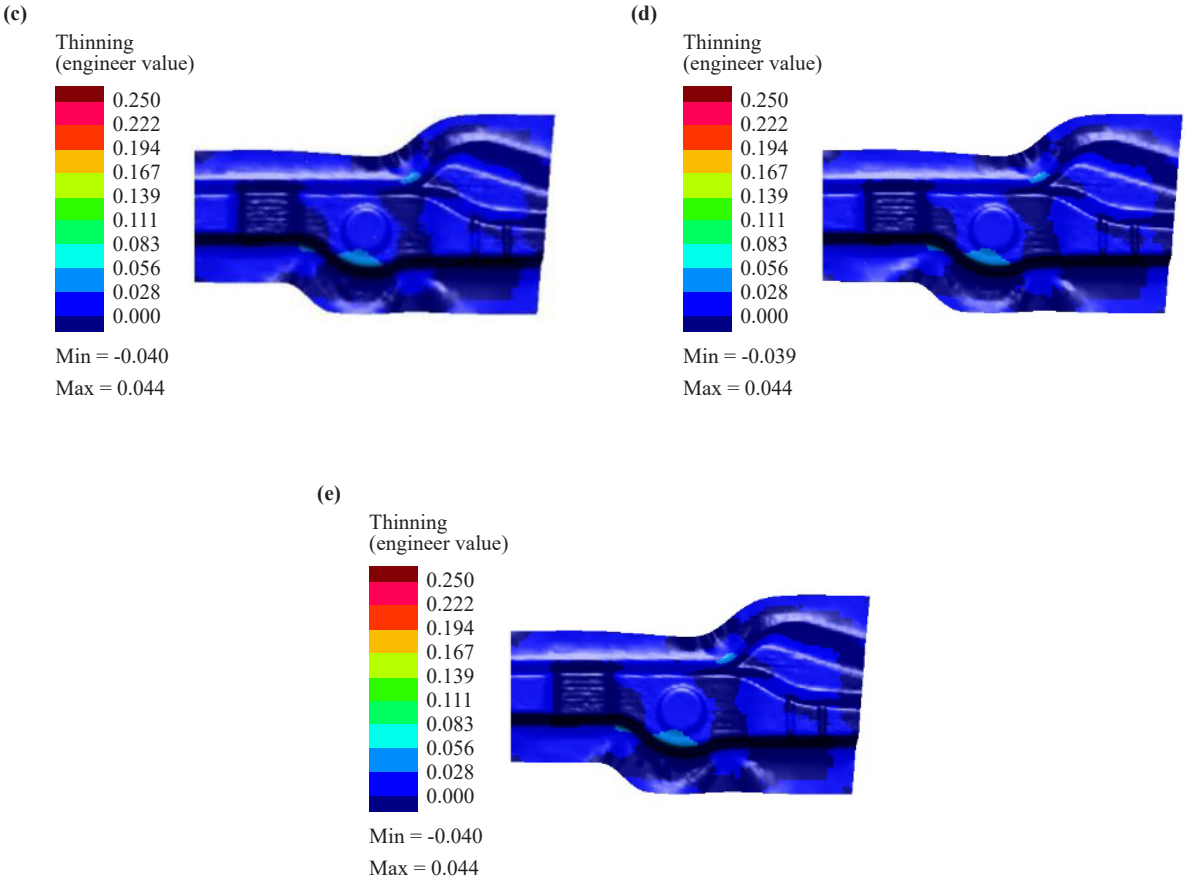

Figure 15. Thinning distribution in cross members for different grades of steel (a) DP 590 (b) DP 780 (c) DP 980 (d) DP 1180 (e) LA 380

For example, high-strength low-alloy (HSLA) steels, such as those in the ASTM A572 grade range, offer excellent strength and toughness, making them well-suited for use in high-stress structural applications [9]. The high strength of these steels allows for thinner cross members, which reduces weight and increases fuel efficiency in vehicles.

Another example is the use of dual-phase (DP) steels, which offer a balance of strength and ductility, making them well-suited for use in automotive applications where high strength and good formability are required. The combination of strength and formability enables thinner cross members to be used, while still maintaining good crash performance.

In comparison, mild steels, such as those in the ASTM A36 grade range, have lower strength and ductility compared to HSLA and DP steels. These steels are typically used in applications where weight and cost are primary concerns, and they generally require thicker cross members to achieve sufficient strength and durability.

It was observed that DP 590 had more elongation percentage compared to other grades of steel, however tensile strength of DP 1180 is the highest among others.

In conclusion, the choice of steel grade will have a significant impact on the thinning distribution in cross members, and the specific requirements of the application, such as strength, toughness, formability, and cost, will dictate the best choice for a given application.

4. Conclusion

This study aims to explore the applicability of various grades of steel in the manufacture of automotive components through finite element simulations using the PAM-STAMP software. To optimize steel grade, five different materials (DP 590, DP 780, DP 980, DP 1180, LA 380) were used for FEM simulation using PAMSTAMP. A room temperature tensile

test was performed for the flow behaviour of these materials, whereas Nakazima test was done for FLD determination. These data were used as input for FEM simulation. Based on the above study, these are the following conclusions.

(i) It was observed that DP 780 had better formability in comparison to other grades of steel.

(ii) Maximum thickness distribution in both the components is higher in the case of DP 590. However, a more uniform thickness distribution was observed in DP 780. It was also observed that as the strength of materials increases formability of materials decreases.

(iii) FLD by Rupture risk criterion indicates that DP 1180 had more chance of failure at a lower strain level.

(iv) FLD of both components indicates that the maximum load distribution is in the drawing region.

(v) It was observed that with an increase in punch velocity formability of the component decreases. However, with respect to the blank-holding force, it can be concluded that the optimum blank-holding force for the above materials is 200 kN. A blank holding force lower than 200 kN produces wrinkling in components whereas a higher blank holding force leads to cracking at a lower strain value.

Data availability

All data generated or analysed during this study are included in this published article (and its supplementary information files).

Conflict of interest

The authors declare no competing financial interest.

References

[1] M. Tisza, *Metal Forming in the Automotive Industry*. Miskolc: University Press, 2020. Available: https://doi.org/10.5772/intechopen.91024.

[2] Lotus Engineering Inc., *An Assessment of Mass Reduction Opportunities for 2017-2020 Model Year Vehicle Programs*. International Council on Clean Transportation, 2010, pp. 308.

[3] P. S. Narayanasamy, A. K. Singh, and K. Narasimhan, "Effect of cooling system in hot stamping process," *IOP Conference Series Materials Science and Engineering*, vol. 967, pp. 012059, 2020.

[4] M. T. Tran, X. M. Nguyen, H. Kim, H. Chae, W. Woo, H. W. Lee, and D.-K. Kim, "Micromechanical properties and deformation behavior of the constituent phases in 3rd generation complex phase AHSS: In-situ neutron experiment and crystal plasticity simulation," *International Journal of Plasticity*, vol. 171, pp. 103812, 2023.

[5] R. Sedaghat-Nejad, H. R. Shahverdi, and M. Askari-Paykani, "Introduction and mechanical evaluation of a novel 3rd-generation medium manganese AHSS with 86 GPa% of PSE," *Materials Science and Engineering: A*, vol. 843, pp. 143104, 2022.

[6] J. Y. Chung, and O. Kwon, "Development of high performance auto steels," in *Proceedings of ICTP 2008*. Gyeongju, Korea, 2008, pp. 3-6.

[7] C. Lesch, N. Kwiaton, and B. Frank, "Advanced High Strength Steels (AHSS) for automotive applications: Tailored properties by smart microstructural adjustments," *Steel Research International*, vol. 88, no. 10, pp. 1700210, 2017.

[8] A. K. Singh, and K. Narasimhan, "Design and development of a micro-LDH apparatus to determine formability of sheet metal under hot stamping conditions using Gleeble," *The International Journal of Advanced Manufacturing Technology*, vol. 123, no. 11-12, pp. 3831-3844, 2022.

[9] T. Nanda, V. Singh, V. Singh, A. Chakraborty, and S. Sharma, "Third generation of advanced high-strength steels: Processing routes and properties," *Journal of Materials: Design and Applications*, vol. 233, no. 2, pp. 209-238, 2019.

[10] A. K. Singh, and K. Narasimhan, "Determination and predication of formability on 22MnB5 steel under hot stamping conditions using Gleeble," *Advances in Materials and Processing Technologies*, vol. 8, no. 2, pp. 1973-1985, 2022.

[11] D. K. Matlock, J. G. Speer, E. De Moor, and P. J. Gibbs, “Recent developments in advanced high strength sheet steels for automotive applications: An overview,” *Journal of Engineering Science and Technology*, vol. 15, no. 1, pp. 1-12, 2012.